Dual optical frequency comb architecture with capabilities from visible to mid-infrared

Borja Jerez,* Pedro Martín-Mateos, Estefanía Prior, Cristina de Dios, and Pablo Acedo

Departamento de Tecnología Electrónica, Universidad Carlos III de Madrid, C/ Butarque 15, 28911 Leganés, Madrid, Spain

bjerez@ing.uc3m.es

Abstract: In this paper, a new approach to dual comb generation based on well-known optical techniques (Gain-Switching and Optical Injection Locking) is presented. The architecture can be implemented using virtually every kind of continuous-wave semiconductor laser source (DFB, VCSEL, QCL) and without the necessity of electro-optic modulators. This way, a frequency-agile and adaptive dual-comb architecture is provided with potential implementation capabilities from mid-infrared to near ultraviolet. With a RF comb comprising around 70 teeth, the system is validated in the 1.5 μm region measuring the absorption feature of $H^{13}CN$ at 1538.523 nm with a minimum integration time of 10 μs.

OCIS codes: (280.4788) Optical sensing and sensors; (140.3520) Lasers, injection-locked; (120.6200) Spectrometers and spectroscopic instrumentation; (300.6310) Spectroscopy, heterodyne.

References and links

1. T. Udem, R. Holzwarth, and T. W. Hänsch, "Optical frequency metrology," Nature **416**(6877), 233–237 (2002).
2. T. Ideguchi, S. Holzner, B. Bernhardt, G. Guelachvili, N. Picqué, and T. W. Hänsch, "Coherent Raman spectro-imaging with laser frequency combs," Nature **502**(7471), 355–358 (2013).
3. T. Udem, "Spectroscopy: frequency comb benefits," Nat. Photonics **3**(2), 82–84 (2009).
4. S. Schiller, "Spectrometry with frequency combs," Opt. Lett. **27**(9), 766–768 (2002).
5. I. Coddington, W. C. Swann, and N. R. Newbury, "Coherent dual-comb spectroscopy at high signal-to-noise ratio," Phys. Rev. A **82**(4), 043817 (2010).
6. F. Keilmann, C. Gohle, and R. Holzwarth, "Time-domain mid-infrared frequency-comb spectrometer," Opt. Lett. **29**(13), 1542–1544 (2004).
7. I. Coddington, W. C. Swann, and N. R. Newbury, "Coherent multiheterodyne spectroscopy using stabilized optical frequency combs," Phys. Rev. Lett. **100**(1), 013902 (2008).
8. B. Bernhardt, A. Ozawa, P. Jacquet, M. Jacquey, Y. Kobayashi, T. Udem, R. Holzwarth, G. Guelachvili, T. W. Hänsch, and N. Picqué, "Cavity-enhanced dual-comb spectroscopy," Nat. Photonics **4**(1), 55–57 (2010).
9. E. Baumann, F. R. Giorgetta, W. C. Swann, A. M. Zolot, I. Coddington, and N. R. Newbury, "Spectroscopy of the methane v3 band with an accurate midinfrared coherent dual-comb spectrometer," Phys. Rev. A **84**(6), 062513 (2011).
10. T. Ideguchi, A. Poisson, G. Guelachvili, N. Picqué, and T. W. Hänsch, "Adaptive real-time dual-comb spectroscopy," Nat. Commun. **5**, 3375 (2014).
11. G. Villares, A. Hugi, S. Blaser, and J. Faist, "Dual-comb spectroscopy based on quantum-cascade-laser frequency combs," Nat. Commun. **5**, 5192 (2014).
12. F. R. Giorgetta, G. B. Rieker, E. Baumann, W. C. Swann, L. C. Sinclair, J. Kofler, I. Coddington, and N. R. Newbury, "Broadband phase spectroscopy over turbulent air paths," Phys. Rev. Lett. **115**(10), 103901 (2015).
13. D. A. Long, A. J. Fleisher, K. O. Douglass, S. E. Maxwell, K. Bielska, J. T. Hodges, and D. F. Plusquellic, "Multiheterodyne spectroscopy with optical frequency combs generated from a continuous-wave laser," Opt. Lett. **39**(9), 2688–2690 (2014).
14. P. Martin-Mateos, M. Ruiz-Llata, J. Posada-Roman, and P. Acedo, "Dual-comb architecture for fast spectroscopic measurements and spectral characterization," IEEE Photonics Technol. Lett. **27**(12), 1309–1312 (2015).
15. P. Martín-Mateos, B. Jerez, and P. Acedo, "Dual electro-optic optical frequency combs for multiheterodyne molecular dispersion spectroscopy," Opt. Express **23**(16), 21149–21158 (2015).
16. V. Durán, S. Tainta, and V. Torres-Company, "Ultrafast electrooptic dual-comb interferometry," Opt. Express **23**(23), 30557–30569 (2015).
17. G. Millot, S. Pitois, M. Yan, T. Hovhannisyan, A. Bendahmane, T. W. Hänsch, and N. Picqué, "Frequency-agile dual-comb spectroscopy," Nat. Photonics **10**(1), 27–30 (2015).
18. A. J. Fleisher, D. A. Long, Z. D. Reed, J. T. Hodges, and D. F. Plusquellic, "Coherent cavity-enhanced dual-

#264266 Received 28 Apr 2016; revised 14 Jun 2016; accepted 20 Jun 2016; published 23 Jun 2016

comb spectroscopy," Opt. Express **24**(10), 10424–10434 (2016).
19. S. Papp, K. Beha, P. Del'Haye, D. Cole, A. Coillet, and S. Diddams, "Self-referencing a CW laser with efficient nonlinear optics," in *Nonlinear Optics,* OSA Technical Digest (Online) (Optical Society of America, 2015), paper NTh3A.6.
20. F. C. Cruz, D. L. Maser, T. Johnson, G. Ycas, A. Klose, F. R. Giorgetta, I. Coddington, and S. A. Diddams, "Mid-infrared optical frequency combs based on difference frequency generation for molecular spectroscopy," Opt. Express **23**(20), 26814–26824 (2015).
21. K. F. Lee, N. Granzow, M. A. Schmidt, W. Chang, L. Wang, Q. Coulombier, J. Troles, N. Leindecker, K. L. Vodopyanov, P. G. Schunemann, M. E. Fermann, P. S. J. Russell, and I. Hartl, "Midinfrared frequency combs from coherent supercontinuum in chalcogenide and optical parametric oscillation," Opt. Lett. **39**(7), 2056–2059 (2014).
22. A. Hugi, G. Villares, S. Blaser, H. C. Liu, and J. Faist, "Mid-infrared frequency comb based on a quantum cascade laser," Nature **492**(7428), 229–233 (2012).
23. S. M. Link, A. Klenner, M. Mangold, C. A. Zaugg, M. Golling, B. W. Tilma, and U. Keller, "Dual-comb modelocked laser," Opt. Express **23**(5), 5521–5531 (2015).
24. J. Chiles and S. Fathpour, "Mid-infrared integrated waveguide modulators based on silicon-on-lithium-niobate photonics," Optica **1**(5), 350–355 (2014).
25. S. Yamashita and G. J. Cowle, "Single-polarization operation of fiber distributed feedback (DFB) lasers by injection locking," J. Lightwave Technol. **17**(3), 509–513 (1999).
26. S. M. Riecke, H. Wenzel, S. Schwertfeger, K. Lauritsen, K. Paschke, R. Erdmann, and G. Erbert, "Picosecond spectral dynamics of gain-switched DFB lasers," IEEE J. Quantum Electron. **47**(5), 715–722 (2011).
27. R. Zhou, T. N. Huynh, V. Vujicic, P. M. Anandarajah, and L. P. Barry, "Phase noise analysis of injected gain switched comb source for coherent communications," Opt. Express **22**(7), 8120–8125 (2014).
28. P. M. Anandarajah, S. P. Ó. Dúill, R. Zhou, and L. P. Barry, "Enhanced optical comb generation by gain-switching a single-mode semiconductor laser close to its relaxation oscillation frequency," IEEE J. Sel. Top. Quantum Electron. **21**(6), 592 (2015).
29. C. H. Chang, L. Chrostowski, and C. J. Chang-Hasnain, "Injection locking of VCSELs," IEEE J. Sel. Top. Quantum Electron. **9**(5), 1386–1393 (2003).
30. A. R. C. Serrano, C. de Dios Fernandez, E. P. Cano, M. Ortsiefer, P. Meissner, and P. Acedo, "VCSEL-based optical frequency combs: Toward efficient single-device comb generation," IEEE Photonics Technol. Lett. **25**(20), 1981–1984 (2013).
31. E. Prior, C. de Dios, Á. R. Criado, M. Ortsiefer, P. Meissner, and P. Acedo, "Experimental study of VCSEL-based optical frequency comb generators," IEEE Photonics Technol. Lett. **26**(21), 2118–2121 (2014).
32. A. Asahara, S. Chen, T. Ito, M. Yoshita, W. Liu, B. Zhang, T. Suemoto, and H. Akiyama, "Direct generation of 2-ps blue pulses from gain-switched InGaN VCSEL assessed by up-conversion technique," Sci. Rep. **4**, 6401 (2014).
33. R. Zhou, S. Latkowski, J. O'Carroll, R. Phelan, L. P. Barry, and P. Anandarajah, "40 nm wavelength tunable gain-switched optical comb source," Opt. Express **19**(26), B415–B420 (2011).
34. N. Jukam, S. S. Dhillon, D. Oustinov, J. Madeo, C. Manquest, S. Barbieri, C. Sirtori, S. P. Khanna, E. H. Linfield, A. G. Davies, and J. Tignon, "Terahertz amplifier based on gain switching in a quantum cascade laser," Nat. Photonics **3**(12), 715–719 (2009).
35. A. K. Wójcik, P. Malara, R. Blanchard, T. S. Mansuripur, F. Capasso, and A. Belyanin, "Generation of picosecond pulses and frequency combs in actively mode locked external ring cavity quantum cascade lasers," Appl. Phys. Lett. **103**(23), 231102 (2013).
36. H. Simos, A. Bogris, D. Syvridis, and W. Elsäßer, "Intensity noise properties of mid-infrared injection locked quantum cascade lasers: I. Modeling," IEEE J. Quantum Electron. **50**(2), 98–105 (2014).
37. C. Juretzka, H. Simos, A. Bogris, D. Syvridis, W. Elsäßer, and M. Carras, "Intensity noise properties of mid-infrared injection locked quantum cascade Lasers: II. Experiments," IEEE J. Quantum Electron. **51**(1), 2300208 (2015).
38. X. Leijtens, "JePPIX: the platform for Indium Phosphide-based photonics," IET Optoelectron. **5**(5), 202–206 (2011).
39. L. A. Coldren, S. C. Nicholes, L. Johansson, S. Ristic, R. S. Guzzon, E. J. Norberg, and U. Krishnamachari, "High performance InP-based photonic ICs—A tutorial," J. Lightwave Technol. **29**(4), 554–570 (2011).
40. P. P. Vasil'ev, I. H. White, and J. Gowar, "Fast phenomena in semiconductor lasers," Rep. Prog. Phys. **63**(12), 1997–2042 (2000).
41. R. T. Ramos, A. J. Seeds, A. Bordonalli, P. Gallion, and D. Erasme, "Optical injection locking and phase-lock loop combined systems," Opt. Lett. **19**(1), 4–6 (1994).
42. E. K. Lau, L. J. Wong, and M. C. Wu, "Enhanced modulation characteristics of optical injection-locked lasers: A tutorial," IEEE J. Sel. Top. Quantum Electron. **15**(3), 618–633 (2009).
43. S. L. Gilbert, W. C. Swann, and C. Wang, "Hydrogen cyanide $H^{13}C^{14}N$ absorption reference for 1530 nm to 1565 nm wavelength calibration - SRM 2519a," Natl. Inst. Stand. Technol. Spec. Publ. 260–137 (2005).

1. Introduction

Although Optical Frequency Combs (OFCs) were first introduced as a powerful metrology tool [1], shortly their potential was widely proven in biomedical applications [2] and spectroscopy [3], among others. In relation to the last field, the current trends based on dual-

#264266 Received 28 Apr 2016; revised 14 Jun 2016; accepted 20 Jun 2016; published 23 Jun 2016

comb spectroscopy [4,5] have proven unprecedented frequency resolution, stability and considerable shrinkage in measurement times in comparison to other state-of-the-art spectroscopic techniques, such as Michelson-based Fourier transform spectroscopy. The principle of operation of dual-comb spectroscopy relies in mapping the modes of two OFCs with slightly different repetition frequencies from the optical domain into the radio-frequency (RF) domain, in order to detect and process the information taking full advantage of the broad variety of techniques and methods available in the latter domain. In this context, traditional dual-comb sources have relied in two-laser schemes and modelocked-based OFCs [6–12]. Nevertheless, the need for synchronization between lasers, restricted repetition frequency, or inherent complexity of these architectures are limitations which usually make these schemes unsuitable to be incorporated in field applications, despite their unassailable capabilities in terms of broadband spectral range and extraordinary precision.

Concurrently, compact OFCs generated by electro-optical modulation of a continuous-wave laser have recently emerged as an attractive alternative when the wide bandwidth of solid-state lasers is not needed [13–18]. Some of the significant features of this approach are the high power of the spectral components (and, hence, higher signal-to-noise ratio –SNR-), simplicity of use and control (including line spacing), and lower cost, which makes them firm candidates to exploit the full potential of dual-comb spectroscopy in real environments. Modest OFCs developed from standard optical devices can be generated with electro-optic modulators including tens of lines [13–15] or, more recently, even hundreds [18]. Additionally, with further expansion stages or the inclusion of highly nonlinear fibres this number can easily reach not only hundreds but even thousands [16,17,19].

Nevertheless, it is the simplicity of these systems, based on commercial telecommunication components, which conveys an additional hindrance which also needs to be overcome. The employment of these components is a restrictive factor in terms of wavelength range of operation, which is mainly centred around 1.5 μm, being impossible, for instance, to reach wavelengths in the mid-infrared (MIR) region, where the presence of strong vibrational bands in a number of gases is well-known. Although MIR optical frequency combs (OFCs) based on different approaches (Difference Frequency Generation –DFG [20]-, optical parametric oscillators –OPOs [21]-), as well as quantum-cascade laser optical frequency combs (QCL-OFCs [22]) have been satisfactorily demonstrated, the advancement of MIR dual OFCs is still in its early stages [11]. Complex structures based on modelocked lasers have already been validated [23], but the lack of consolidated and robust electro-optic modulators in this spectral range (can be found from 400 nm up to 2 μm) [24] confirms that there is still work ahead until dual combs are seamlessly integrated in the MIR, as direct translations of the compact architectures already demonstrated at 1.5 μm are not possible.

In this paper, we introduce a completely new approach to dual-comb sources which intends to overcome the aforementioned drawbacks by combining Gain-Switched Optical Frequency Combs (GS-OFCs) with Optical Injection Locking (OIL). These two techniques have been separately or in conjunction used with different continuous-wave semiconductor laser sources (DFBs [25–28], VCSELs [29–32], Fabry-Pérot LDs [33], QCLs [34–37]) in the complete wavelength range from MIR to visible. This way, it is possible to combine them to implement compact, real-time, high-resolution and versatile dual-comb architectures whose capacity can be uninterruptedly exploited not only in NIR but also in adjacent regions of the electromagnetic spectrum.

Moreover, this compact architecture can be integrated using already accessible and validated PIC (Photonic Integrated Circuit) technologies using generic platforms [38,39], providing with a potentially low-cost solution to take these systems outside the research laboratories and expand the capabilities of ultra-high resolution dual-comb spectroscopy to other application fields where high resolution spectral characterization is required, from optical fibre sensors interrogation to biomedical applications.

#264266 Received 28 Apr 2016; revised 14 Jun 2016; accepted 20 Jun 2016; published 23 Jun 2016

2. Gain-Switching injection-locked dual-comb architecture

2.1. Compact dual-comb architecture description

The proposed scheme of the dual-comb spectrometer is depicted in Fig. 1. The optical power of a continuous-wave laser diode (which henceforth will be denominated as master) is divided into two optical paths to inject a new pair of laser diodes (slaves). Before splitting the optical power of the master, an isolator is placed to quench unwanted feedback reflections. In order to generate OFCs, both injected slaves are directly modulated through Gain-Switching at slightly different repetition frequencies. These frequencies can be uncomplicatedly tuned by signal generators. Additionally, to cancel mode averaging, one of the OFCs is frequency-shifted with an acousto-optic modulator (AOM) [13]. After polarization matching, both OFCs are combined.

Before being heterodyned on a photodetector, the combined OFCs can either traverse the device under test (DUT) to be characterized or serve as a reference. The resultant periodic interferogram (and the subsequent RF comb after Fourier transformation) is then bandpass-filtered (in order to discard higher order RF combs) to be digitized by an acquisition system afterwards. Finally, a multitone parallel detection scheme with adaptable configuration for ultra-high speed measurements allows recovering the amplitude and the phase of the spectral components in each RF comb.

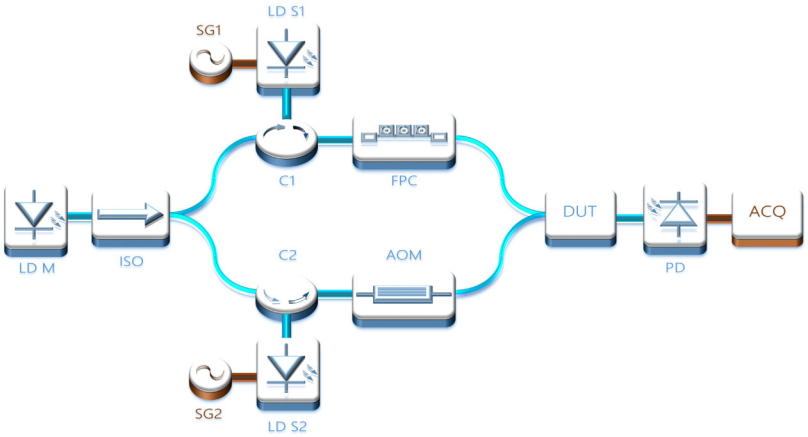

Fig. 1. Experimental setup of the spectrometer. LD M: Laser diode master; ISO: Optical isolator; C1/C2: Circulators; LD S1/2: Laser diode slaves; SG1/2: Signal generators; AOM: Acousto-optic modulator; FPC: Fibre polarization controller; DUT: Device under test; PD: Photodetector; ACQ: Acquisition system.

2.2. Gain-Switching

The principle of operation of Gain-Switching consists of a periodic and sudden switching of the laser gain [40]. In our experiment, this is accomplished by biasing the laser with an electrical current (I_{bias}) and applying a large continuous-wave signal that modulates the laser (I_{RF}), thus producing a pulsed optical output. This modulation and bias are coupled to the diode laser thanks to a bias-tee element integrated into the laser case. The result in the optical domain is an asymmetric OFC with line spacing equal to the frequency which directly modulates the laser bias current (f_{REP}). Since the number of teeth generated depends on the ratios I_{RF}/I_{bias}, I_{bias}/I_{TH} (where I_{TH} refers to "threshold current") and f_{REP}, a meticulous experimental study of these parameters was carried out for a set of fixed modulation frequencies (up to 12 GHz). Continuous measurements for bias currents ranging from the threshold current up to its maximum (following specifications) were performed for a batch of different modulation powers in order to achieve the best OFCs according to two figures of

#264266 Received 28 Apr 2016; revised 14 Jun 2016; accepted 20 Jun 2016; published 23 Jun 2016

merit: number of optical lines and flatness of the OFC. All lasers were stabilized in current and temperature with standard laser diode controllers.

2.3. Optical injection locking

The process of optical injection relies in the injection of the output optical field of a laser (which is usually denominated as master) into the cavity of a secondary (or slave) laser. Locking takes place when the frequencies (or emission wavelengths) of the master and slave are proximate enough, within the locking range. Therefore, the slave is obliged to perform on the injected wavelength along a certain locking range. In this case, since the optimum bias current of the slave lasers is established in accordance with Gain-Switching operation, a temperature tuning was carried out to adjust their wavelength emission roughly into the vicinity of the molecular transition of interest. With regard to the master, its output power was set about ~10 dB above the output power of the slave lasers (injection ratio) and its wavelength emission was also controlled acting over its temperature. Fibre polarization controllers placed between master and slaves enabled additional control over the injection locking mechanism. An example of the resultant OFC (before combination) is shown in Fig. 2, where the injection of the master laser in one of the teeth of the gain-switched slave lasers is appreciable in the optical spectrum. The proper performance of the injection locking technique is ensured by two facts. First, the ultra-narrow linewidth of the master and slave lasers (Master ≈34 kHz; Slave 1 ≈54 kHz; Slave 2 ≈367 kHz) that prevent the interaction of the master with adjacent comb lines. Second, the locking range is below the repetition frequency of the comb for the injection ratio considered in our experiment.

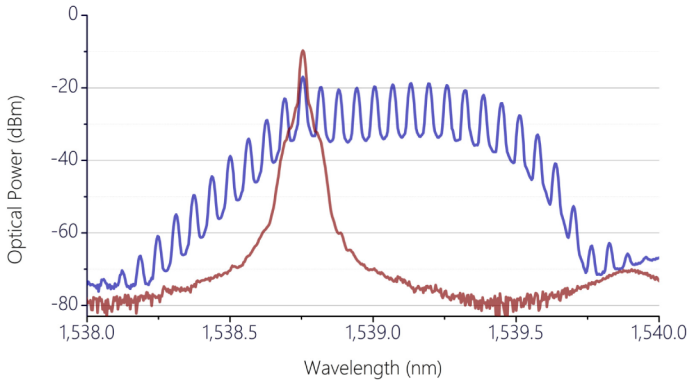

Fig. 2. Example of Gain-Switching optical injection locking. The red line shows the master laser. After optical injection of the slave laser, a pulsed optical regime is induced in it using gain switching and, consequently, an OFC is generated (blue line). The injection of the master in one of the teeth of the OFC is discernible. In this example, the wavelength emission is fixed at 1538.75 nm and the repetition frequency of the OFC at 8 GHz. The spectra is measured in an optical spectrum analyser with 20 pm resolution.

2.4. Processing techniques: Acquisition of the interferogram

The processing method is based on the Fourier transformation of the time-domain interferogram (see Fig. 3). A multichannel digital lock-in detection system implemented in Matlab (developed and detailed in previous work [14]) features flexible configuration in terms of number of channels, integration time and reference frequencies. The RF combs digitized are processed in parallel allowing simultaneous characterization of multiple spectral points. The reference frequency of each channel can be set to coincide with the frequencies of the lines of the RF comb, thus allowing each channel to be analysed concurrently in order to extract the amplitude of each component of the comb. The integration time for each channel is also adaptable, only restricted by its minimum value, which is inversely proportional to the spacing between the repetition rates. Along with an increase in integration time, additional

#264266 Received 28 Apr 2016; revised 14 Jun 2016; accepted 20 Jun 2016; published 23 Jun 2016

low-pass filtering can also be carried out to smooth the final result or to diminish the impact of haphazard environmental effects when the application is not time-critical.

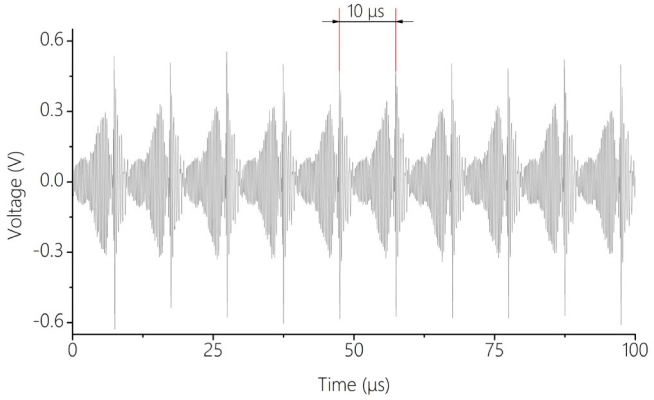

Fig. 3. Time-domain interferogram for a measurement time of 100 µs. The space between two consecutive pulses corresponds to the inverse of the difference in the repetition frequencies (in the example illustrated, 100 kHz)

2.5. Additional considerations

In this point, there are a few noteworthy aspects of the system which must be highlighted. Firstly, since one single laser (master) drives both OFCs, the need for synchronization is dismissed and amplitude and phase fluctuations of the laser are also self-compensated. Additionally, a similar outcome can be gleaned from OIL: when phase-locking between both master and slave takes place, the slave is obliged to follow the track of any phase fluctuation which occurs in the master [41]. Further benefits in terms of performance can also be attained when the locking is stable, such as laser spectral narrowing, frequency chirp decrement or noise reduction [42]. Other collateral advantages of the proposed system are the lower influence of Flicker noise as a result of the inclusion of a non-compulsory AOM, which centres the RF comb at its modulation frequency, or its improved robustness and versatility for spectral characterization, since the configuration of the dual-comb architecture does not have any effect on the DUT per se. On top of that, and as mentioned before, all these features can be promptly transferred to other spectral regions.

3. Experimental validation

The proficiency of the presented architecture is validated with the measurement of the ro-vibrational transition of $H^{13}CN$ at 1538.523 nm [14,17]. For this purpose, the DUT comprises a 55 mm length gas cell filled with $H^{13}CN$ at 100 Torr (HCN-13-H(5.5)-100-FCAPC, Wavelength References Inc.) together with an optical switch (OSW-2X2BA, Fiberstore Inc.) which allows the OFC to bypass the cell and therefore obtain a reference RF comb without the need of a second photodetector, also avoiding imbalances between the signal and reference paths and improving the SNR in 3 dB. For this purpose, the scheme encompasses three Discrete Mode laser diodes (EP 1538-5-DM-H19-FM, Eblana Photonics Ltd.) emitting around 1538.5 nm. The emission wavelength was tuned by means of the temperature and bias current of the laser controller (the tuning range of the lasers is around 4 nm). The optical power of the master was divided into two paths (50/50 optic coupler), which eventually could be regarded as the two arms of an interferometer. Two identical circulators allowed the injection in both slave lasers to take place, which were simultaneously modulated through GS at a frequency of 1 GHz and 1.0001 GHz, respectively. One of the OFCs was launched into an acousto-optic modulator (T-M040-0.5C8J-3-F2S, Gooch and Housego PLC) driven at 40 MHz with a RF power around 24 dBm to ensure that each spectral feature in the optical domain is unequivocally mapped into the RF domain. A fibre polarization controller

#264266 Received 28 Apr 2016; revised 14 Jun 2016; accepted 20 Jun 2016; published 23 Jun 2016

(FPC030, Thorlabs Inc.) was introduced in one path to control the polarization state of the optical beams so that both OFCs had parallel linear states of polarization before combining. One InGaAs transimpedance photodetector (PDA10CF, Thorlabs Inc.) was placed to detect the reference and signal combs. The resultant RF combs were bandpass-filtered with standard RF filters (SIF-40 + , Mini-Circuits Inc.) and digitized with a 14-bit waveform digitized board (PDA14, Signatec Inc.). The RF signals were synchronously subsampled at 36 MS/s, thus displacing the comb to normalized frequency equivalent to 4 MHz while preserving the repetition rate. The generation of all RF signals (slave lasers modulation, AOM modulation and acquisition clock) were carried out by the same phase coherent synthesizer (HS9004A, Holzworth Instrumentation Inc.). No active temperature stabilization or vibration isolation procedures were implemented.

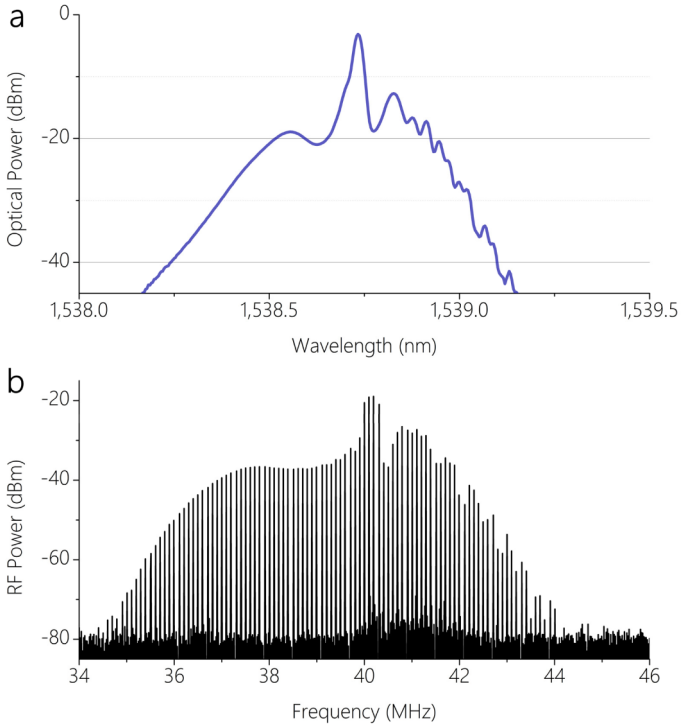

Fig. 4. Gain-switched injection-locked dual combs. a) Optical domain. Around 70 lines spaced 1 GHz (which corresponds to ~0.55 nm) into the 20 dB span. No expansion stages were included in the setup. b) RF spectra of the comb obtained after Fourier-transforming the signal heterodyned on the photodetector. The central line has the frequency which drives the acousto-optic modulator (40 MHz). The rest of modes are located at higher and lower frequencies asymmetrically due to the intrinsic properties of Gain-Switching in the lasers. The separation between lines (ergo, separation between repetition rates) is fixed at 100 kHz.

The combs generated with this approach (optical and RF domain) are illustrated in Fig. 4. With the GS ratios fixed at I_{RF}/I_{bias} = 1.8, I_{bias}/I_{TH} ≈4, the repetition frequencies set at 1 GHz and the separation between them at 100 kHz (which leads to a periodicity in the interferograms of 10 μs), the resultant OFC (Fig. 4(a)) contains around 70 lines into the 20 dB span without introducing any sort of expansion stage. This number of lines is two or three times higher than similar schemes with a single expansion stage [13,14]. The comb obtained in the RF domain resulting after the downconversion from the optical domain is shown in Fig. 4(b). Additionally, the linewidth of one RF comb line has been evaluated with a spectrum analyzer. As we have observed, the 3 dB linewidth is below the resolution of the device (Resolution Bandwidth = 1 Hz). This is a clear indication of the extremely high coherence between both injection-locked OFCs.

#264266 Received 28 Apr 2016; revised 14 Jun 2016; accepted 20 Jun 2016; published 23 Jun 2016

After processing, the resultant trace representing the ratio between the amplitudes of the measurement and reference combs is shown in Fig. 5 together with a Voigt fit for four different integration times: 10 μs (the minimum value, as the difference between repetition rates is 100 kHz), 50 μs, 100 μs and 500 μs. Additionally, a plot including an average of 20 spectra with an integration time of 20 ms is presented. In this case, the residuals between the experimental spectra and the Voigt fit show a standard deviation of 0.57%. The peak absorption of ~1.07 dB at the centre wavelength and linewidth of ~8 GHz denotes excellent agreement with the expected result [43], while the measurement time is in line with the expected ultra-high speed spectroscopic measurement capabilities of the spectrometer. The noise-equivalent absorption (NEA), defined as $(L_{abs}\ SNR)^{-1}(T/M)^{1/2}$, is 6.87×10^{-6} cm^{-1} $Hz^{-1/2}$ at 1 s averaging, where L_{abs} = 5.5 cm, SNR = 100, T = 1 ms and M = 70.

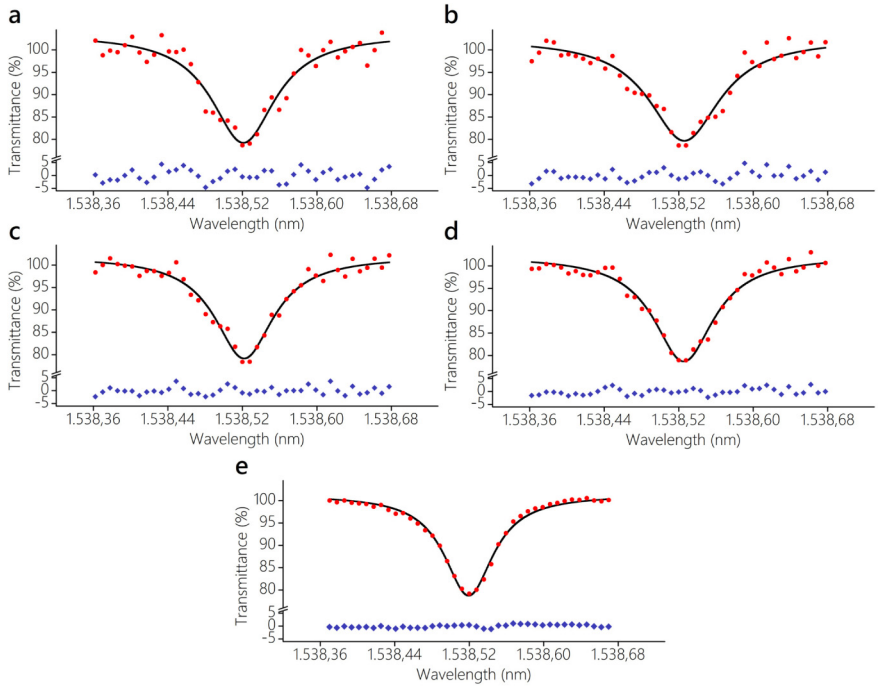

Fig. 5. Experimental validation in the 1.5 μm region. The dots represent the trace of the measured ro-vibrational transition presenting the R(5) line of the 2v3 band of $H^{13}CN$ for different measurement times along with the residuals: a) 10 μs; b) 50 μs; c) 100 μs; d) 500 μs; e) Average of 20 spectra measured over 20 ms. The continuous line shows the Voigt fit of the results, leading to standard deviations between the experimental data and the fit of: a) 2.34%; b) 1.89%; c) 1.49%; d) 1.27%; e) 0.57%. A bottom value for the transmittance of 78% (which corresponds to a peak absorption of 1.07 dB) is quantified at the centre of the spectral line, along with a linewidth around 8 GHz. These values agree with the standard values reported in the NIST SRM 2519a.

4. Conclusions

We have introduced for the first time a compact dual-comb architecture whose performance relies in Gain-Switching, to induce pulsed operation in the lasers and consequently generate OFCs with slightly different frequency spacing without the necessity of electro-optic modulators, and optical injection locking to synchronize them. The presented system maintains the range of advantages of classical electro-optic dual optical frequency comb configurations, such as high resolution, spatial coherence, ultrafast speed of operation and ease control of mode spacing but, at the same time, the GS approach permits the generation of

#264266 Received 28 Apr 2016; revised 14 Jun 2016; accepted 20 Jun 2016; published 23 Jun 2016

OFCs without using wavelength-restrictive optical components. Finally, OIL yields coherence between OFCs and additional benefits in the performance of the system.

The GS-OIL dual-comb architecture is firstly validated in the NIR region, but since all these components and techniques have already been demonstrated in the MIR and visible ranges successfully, the deployment to these regions is straightforward. In conclusion, the presented architecture, on one hand, paves the way for compact dual-comb MIR spectroscopy by taking full advantage of simple schemes and commercially available components, and, on the other hand, provides a compact, integrable (using standard PIC technology) and potentially low-cost solution to, firstly, take these systems outside the research laboratories and, secondly, to expand the capabilities of ultra-high resolution dual-comb spectroscopy to other application fields where high resolution spectral characterization is required, from optical fibre sensors interrogation to biomedical applications.

Acknowledgments

The authors would like to thank the Spanish Ministry of Economy and Competitiveness for supporting the projects under the RTC-2014-2661-7 and TEC-2014-52147-R. The work by Borja Jerez has been performed in the frame of a FPU Program, #FPU014/06338, granted by the Spanish Ministry of Education, Culture and Sports.

#264266 Received 28 Apr 2016; revised 14 Jun 2016; accepted 20 Jun 2016; published 23 Jun 2016